Soft Matter

PAPER

View Article Online
View Journal | View Issue

The viscosity of short polyelectrolyte solutions

Cite this: *Soft Matter*, 2014, **10**, 1714

Dora Izzo,*[a] Michel Cloitre[b] and Ludwik Leibler[b]

We consider the viscosity of solutions of highly charged short polyelectrolytes. Our system is a poly(styrene–maleic acid) copolymer solution (SMA) with various added salt concentrations in dilute and semidilute regimes. The SMA solutions show some particular features: (i) variations of the specific viscosity measured for different values of concentration and ionic strength can be rescaled on two universal curves when plotted as a function of the effective volume fraction; (ii) the reduced viscosity is proportional to the Debye length. In order to describe the viscosity of such a system we model the motion of the charged rods considering a simpler system: we replace each charged rod and its corresponding charge cloud by an effective neutral rod. This modified system is yet below the concentrated regime and, at most, steric interactions are left. In the semidilute regime, we model the rescaled rods moving under a mean field potential and obtain a dynamical equation for the orientational tensor, considered small, and the viscosity is derived from it. Within our mean field approach, the effects due to the rod Brownian motion and due to the potential cancel each other and the behavior of the viscosity is explained in terms of the effective volume fraction only. Our predictions are in good qualitative agreement with the experimental results over a wide range of parameters, and suggest a method for obtaining the rotational diffusion constant in the semidilute regime.

Received 11th October 2013
Accepted 9th December 2013

DOI: 10.1039/c3sm52630e

www.rsc.org/softmatter

1 Introduction

Polyelectrolytes are known to exhibit anomalous viscosity properties when compared to neutral polymers. Consider the following experiments: in the first one, we dissolve a neutral polymer in a good solvent; in the second, we dissolve a charged polymer in a polar solvent. Suppose the molecular weight of the chains and the polymer concentrations are the same. The increase in viscosity is much more pronounced in the second case than in the first one. This phenomenon is called the polyelectrolyte effect, and it results both from intra- and inter-chain long range electrostatic interactions.

Many experimental and theoretical efforts have been devoted to study the viscosity of solutions of high molecular mass polyelectrolytes. Since the early 50's, the empirical Fuoss law[1–3] has been used to describe the viscosity of semidilute solutions, although in many situations more complicated behavior has been reported.[4,5] Despite a considerable theoretical effort, the interpretation of the viscosity of long polyelectrolytes is still a highly controversial issue.[6]

In contrast, short polyelectrolytes have been much less studied. Yet, short polyelectrolytes appear to be of growing interest in industrial applications. For example, they tend to replace classical surfactants in the stabilization of emulsions, lattices and mineral colloids. As a consequence, a large variety of low molecular weight polyelectrolytes have been synthesized and patented during the last two decades; among them one finds statistical and block copolymers containing both hydrophobic and hydrophilic monomers. A considerable effort has been devoted to study the interfacial properties, stabilization efficiency and detergency[7] of such systems. However, much less is known about their viscosity. From the fundamental point of view, the flow behavior of short chains is also very interesting.[8] Indeed, one does not expect significant changes in the chain conformation; moreover one looks for information on inter-chain interactions and on the coupling between the motion of polyions and the flow of small ions. This could help for a better understanding of the viscosity of polyelectrolytes in general.

The main aim of this work is to investigate the interaction between the charged short rod like colloids and the fluid flow. This paper reports the study of the viscosity of solutions of very low molecular mass highly charged linear polyelectrolytes with a polymerization index of around 25. For such polyions, the persistence length l_p can be considered of the order of the extended chain length L, and therefore rather small variations of their conformation are expected when polymer and salt concentrations are varied: they can be considered as stiff charged rods. In the dilute and semidilute regimes, the solution viscosity dependence on polymer and added salt concentrations is qualitatively similar to that of high molecular mass polyelectrolytes. This behavior is neither due to conformational changes (since chains are short) nor due to long-range cooperative dissipative effects (since one is below the concentrated

[a]*Instituto de Física da Universidade Federal do Rio de Janeiro, Caixa Postal 68528 21941-972, Rio de Janeiro, Brazil. E-mail: izzo@if.ufrj.br; Fax: +55 21 2562 7368; Tel: +55 21 2562 7895*

[b]*Matière Molle et Chimie E.S.P.C.I., 10 rue Vauquelin 75231, Paris, France*

limit). We propose a mechanism to explain the experimental data: each charged rod and the corresponding stiff double layer are replaced by an effective stiff enlarged neutral rod. At the highest concentrations studied here, we consider that the rods move under a mean field potential due to excluded volume interactions averaged over the rod distribution.

We assume the fluid is Newtonian (to be verified experimentally) and look for an expression for the stress tensor. A calculation well described in the literature (reviewed here)[9,10] decouples the total stress into a viscous and an elastic contribution. A few approximations yield an expression for the total stress as a function of the fluid velocity gradient. The viscosity is then extracted; it has a very simple form, similar to the one for the corresponding neutral system.[9] By studying numerically the expression for the coefficient of viscosity, we arrive at several predictions, including the dependence of the specific viscosity on the polymer concentration and that of the reduced viscosity on the Debye length. Predictions are in qualitative agreement with the experimental results.

The paper is organized as follows. Section 2 gives an overview of the experimental results on the viscosity of long electrolytes. The experimental conditions are described in Section 3. In Section 4 we characterize the system and discuss the data obtained. In Section 5 we make a review of the theoretical framework and obtain a closed expression for the viscosity of charged rod like colloids under fluid flow; at the end of this section we present our predictions. A comparison between experimental results and theoretical predictions with conclusions is left for Section 6.

2 Viscosity of long polyelectrolytes: experimental results

The viscosity of solutions of long polyelectrolytes presents very particular behavior when compared to their neutral analogues. This was first reported by Fuoss[1–3] who used an empirical law to fit the dependence of the reduced viscosity,

$$\eta_{\mathrm{red}} = \frac{\eta - \eta_{\mathrm{s}}}{c\eta_{\mathrm{s}}}, \qquad (1)$$

as a function of polyelectrolyte concentration. In the expression, η and η_{s} are the solution and solvent viscosities respectively and c is the polymer concentration, expressed in mass per unit volume.

Fuoss measurements were performed in dilute solutions, with and without salt. In the case of no salt added, he was able to fit his data by

$$\eta_{\mathrm{red}} = \frac{A}{1 + Bc^{1/2}}, \qquad (2)$$

where A and B are constants; later, it was found that they are functions of the chain total charge.[11] For the smallest concentrations he measured, this function assumes an asymptotic form, $\eta_{\mathrm{red}} \sim c^{-1/2}$; that is, in the absence of salt, the data show a divergence at low c's. In the presence of salt, no such divergence was observed. This type of behavior was found in similar systems, for instance by Prini and Lagos[12] and more recently by Vink,[13] who observed that for a given polyelectrolyte, the rise gets more pronounced as the chain length increases. In 1954, Eisenberg and Pouyet[14] extended viscosity measurements to smaller concentrations (two orders of magnitude down) and found a maximum in η_{red} as a function of the polymer concentration. Later Cohen *et al.*[15] made very careful measurements investigating the behavior of this peak; they established that the concentration at the peak is proportional to the added salt concentration and that it disappears as enough salt is added to the solution; they suggested a phenomenological expression to account for the increase in viscosity with the concentration on the left side of the peak: $\eta_{\mathrm{red}} \sim c$. This change in behavior at the peak points the onset of interpolyion interactions.

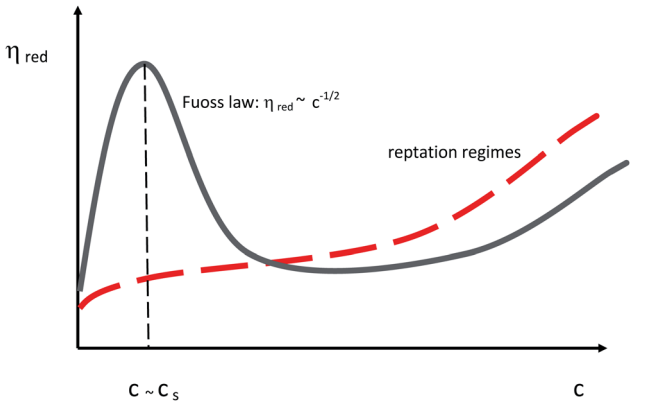

Fig. 1 Draft of the behavior of the reduced viscosity as a function of the polymer concentration. Continuous curve: no salt added; dashed curve: high salt condition.

We summarize this discussion as follows. In the absence of salt, a series of concentration regimes exist: at very low concentrations (left side of the peak), the reduced viscosity is an increasing function of c, being well characterized by isoionic dilution curves; as the polymer concentration reaches a value comparable to the salt concentration, a peak is observed; on the right side of the peak, the Fuoss regime sets in, where $\eta_{\mathrm{red}} \sim c^{-1/2}$, the Fuoss regime corresponds to the semidilute unentangled regime; with increasing concentration, a sequence of reptation regimes follows, where $\eta_{\mathrm{red}} \sim c^{y}$, with $y \geq 1/2$, extensively studied in ref. 5 and 12 and by Dou and Colby as reported by Dobrynin and Rubinstein.[16] In the case of high salt concentrations, no peak is observed; in the semidilute unentangled regime, $\eta_{\mathrm{red}} \sim c^{1/4}$ as described by Boris and Colby;[5] in the semidilute entangled regime, recent experiments by Oelschlaeger *et al.*,[17] suggest $\eta_{\mathrm{red}} \sim c^{3}$. In Fig. 1 we present a summary of these findings, as suggested in ref. 6.

3 Experimental section

3.1 Preparation of styrene–maleic and acid copolymers

The styrene–maleic and acid copolymers used in this study are prepared from styrene–maleic anhydride (SMA1000) commercially available from Xitran. The mass density of the polymer is $\rho_{\mathrm{p}} = 1.3$ g cm^{-3}. Styrene–maleic anhydride is a powder

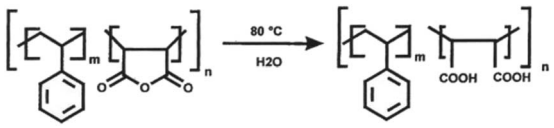

Fig. 2 Maleic-anhydride functions hydrolyzed into maleic acid.

insoluble in water at room temperature. We proceed as follows. Styrene–maleic anhydride is first dispersed in ultrapure water (milli-Q grade) and stirred vigorously for 30 minutes. Then the required amount of NaOH (Titrisol) and eventually NaCl are added to the suspension. The mixture is maintained at 80 °C for 6 hours under stirring. During this thermal treatment, maleic anhydride functions are hydrolyzed into maleic acid (Fig. 2).

Carboxylic groups are ionized depending on the amount of sodium hydroxide added to the solution. To quantify the neutralization of the polymer, we use the degree of neutralization α, which is the ratio of the number of moles of base added to the solution to the number of moles of acid groups available. Similarly, the quantity of NaCl salt in the solutions is characterized by the total molar concentration. The polymer concentration in solution C_p is expressed in terms of the weight fraction (g g^{-1}).

3.2 Measurements

The densities of the solutions at different concentrations are determined with a pycnometer. Conductivity and pH measurements were performed to relate the actual ionization degree of styrene–maleic acid solutions to the neutralization degree. The conductimeter was a Metrohm 712 and the pH-meter was a Metrohm 691. Experiments were performed in sealed cells after carefully degassing the solutions with nitrogen.

The viscosities of the solutions were measured using an Ubbelohde capillary viscometer (Schott Geräte 0a). Each experiment was repeated 6 times. The accuracy in the average flow time was about 0.2 s. The lowest flow time, which was measured for pure water, was equal to 181 s. All the solutions were supposed to be Newtonian at the shear rates encountered in the Ubbelohde viscometer. For the most concentrated solutions (up to 0.05 g g^{-1}) we used a stress controlled rheometer Haake Rs 150 equipped with a double Couette geometry. The results confirmed that the viscosity does not depend on the shear rate.

3.3 Characterization of copolymers

The molecular weight of SMA1000, determined by Size Exclusion Chromatography (SEC) in tetrahydrofuran, was found to be $M = 2500$ g mole^{-1} with a polydispersity of 2.5. The ratio between the number of styrene (S) units and that of maleic anhydride (MA) units, S/MA, is determined by ^{13}C nuclear magnetic resonance (NMR) spectroscopy:[18] it is equal to 1.15. Using the molar mass of styrene (106 g mole^{-1}) and maleic anhydride (116 g mole^{-1}), we deduce that a SMA molecule contains 10 maleic anhydride units and 11 styrene units in average. Concerning the arrangement of the units along the chain, the analysis of the NMR spectra reveals that most of the triads can be assigned to MA–S–MA sequences indicating alternation of S and MA units along the chain.

We have also characterized the properties of styrene–maleic acid solutions. The solution mass densities vary from $\rho = 1.00$ g cm^{-3} at very low concentrations ($C_p = 0.001$ g g^{-1}) to $\rho = 1.03$ g cm^{-3} at the largest concentrations investigated ($C_p = 0.1$ g g^{-1}). These values are useful when one converts the experimental concentration into the polymer volume fraction in solution. The pH of the solution is roughly constant below $\alpha = 0.6$ and increases sharply above this value. Therefore only one half of the available carboxylic functions are effectively ionized in the presence of an excess of base. This observation is associated with the fact that counterions are condensed on the chain at high neutralization degrees.[18] Counterion condensation occurs because the distance between two carboxylic functions carried by the same maleic unit is of the order of the Bjerrum length $l_B = 0.7$ nm. However, conductimetry measurements and neutron scattering experiments show that condensation is still negligible at $\alpha = 0.5$, so that the ionization degree can be considered equal to the neutralization degree.

3.4 Styrene–maleic acid solutions as charged rod solutions

The chemical structure of SMA molecules produces quite a rigid structure, and one expects a persistence length of the order of the chain length. Therefore we can take styrene–maleic acid molecules as rigid rods. In the following, the length of a rod will be taken equal to the length of the molecules in the fully extended conformation: $L = 6.5$ nm. The volume of the rod ν is deduced directly from the molar mass density

$$\nu = \frac{M}{N_A \rho_p}, \quad (3)$$

where N_A is the Avogadro number. We find $\nu = 3.3$ nm^3 and deduce the diameter of the rod $b = 0.8$ nm and the aspect ratio $L/b = 8$. It is convenient to express the rod concentration by the number of rods per unit volume $n = \rho C_p \frac{N_A}{M}$.

As far as we know, no theory predicts concentration regime boundaries for a system of stiff finite charged rods. In a system of neutral finite rods, the dilute regime takes place for $L \leq n^{-1/3}$, so that each rod can rotate freely. In the semidilute regime, $L \geq n^{-1/3} \gg (L^2 b)^{1/3}$; the dynamics is entirely different from the previous one due to entanglement effects: rotation is hindered. If our rods were neutral, the upper concentration limits for the dilute regime and semidilute regimes would be $C_p \simeq 0.015$ g g^{-1} and $C_p \simeq 0.12$ g g^{-1} respectively. The presence of charges will effectively bring these limits down (to be verified experimentally), therefore we conclude that here we span the dilute and semidilute regimes.

In solutions, SMA rods bear an electric charge. Since $\alpha = 0.5$, one half of the carboxylic functions carried by the maleic acid units are ionized, each rod carries 10 electrons in average.

To obtain the Debye screening length, we suppose that all the ions present in the solution contribute to screen the potential. These are:

(i) the counterions associated with the fixed charges carried by the rods. Their concentration is expressed by the number density $n_c = 10$ n, because there are 10 charges per rod;

(ii) the ions coming from the salt (NaCl) added to the solution. Their concentration is given by the number density $n_s = 2000c_sN_A$, where c_s is the salt concentration in mole l^{-1} and

(iii) the ions originally present in the water used to prepare the solutions. Their number density is $n_r = 2000c_rN_A$, where $c_r = 3 \times 10^{-5}$ mole l^{-1} is the residual salt concentration, measured by conductivity. The corresponding expression for the Debye length λ_D is

$$\lambda_D = [4\pi l_B(n_c + n_s + n_r)]^{-1/2}, \quad (4)$$

where $l_B = e^2/4\pi\varepsilon k_BT$ is the Bjerrum length.

4 Results and discussion

4.1 Viscosity of solutions *versus* the polymer concentration and salt concentration

The specific viscosity is defined as

$$\eta_{sp} = \frac{\eta - \eta_s}{\eta_s}, \quad (5)$$

where η and η_s are the solution and solvent viscosities respectively.

In Fig. 3, we show the measured specific viscosity as a function of the redefined volume fraction ϕ_{eff}:

$$\phi_{eff} = n\frac{4}{3}\pi\left(\frac{L + \beta\lambda_D}{2}\right)^3, \quad (6)$$

the effective volume fraction, where β is a parameter used to fit the experimental data. At every C_p, various measurements for different c_s's were made. Using $\beta = 0.125$, we observe that the data plotted for varying ionic strengths fall onto two universal curves (straight lines) with distinct slopes.

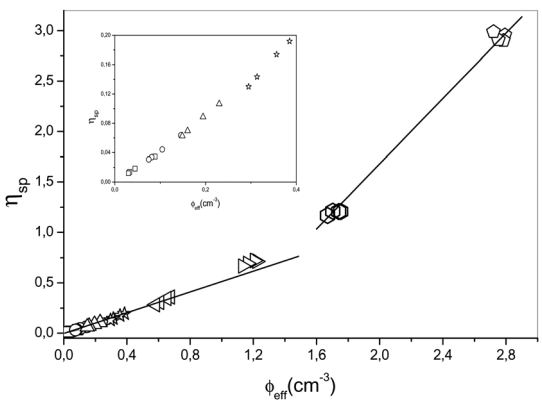

Fig. 3 Measured specific viscosity *versus* effective volume fraction. For every C_p, there is a set of decreasing η_{sp} corresponding to c_s = 0.00 mol l^{-1}, 0.01 mol l^{-1}, 0.05 mol l^{-1} and 0.1 mol l^{-1}. Squares: C_p = 0.001 g g^{-1}; circles: C_p = 0.0025 g g^{-1}; up triangles: C_p = 0.005 g g^{-1}; stars: C_p = 0.01 g g^{-1}; left triangles: C_p = 0.02 g g^{-1}; right triangles: C_p = 0.04 g g^{-1}; hexagons: C_p = 0.06 g g^{-1} and pentagons: C_p = 0.01 g g^{-1}. The inset shows the details in the low C_p region ($C_p \leq 0.01$ g g^{-1}). The two lines indicate different slopes.

This figure shows that there are two distinct regions: one for $C_p \leq 0.02$ g g^{-1} and other for $C_p \geq 0.06$ g g^{-1}. This suggests that up to $C_p = 0.02$ g g^{-1} interactions between rods are unimportant; this coincides with our previous estimate of the boundary between dilute and semidilute regimes (Section 2.4). It is interesting to note that, in the case of neutral rods, in the dilute limit, the dependence of the η_{sp} on the bare volume fraction ϕ is also linear.[9]

In order to compare the reduced viscosity of these short charged rods with their long flexible analogues (described in Section 2), we show in Fig. 4 a plot of the reduced viscosity as a function of the polymer concentration. In general we observe the polyelectrolyte effect: the viscosity goes down with increasing salt concentration; at higher polymer concentrations, addition of salt is irrelevant. In the absence of the salt condition, well in the dilute regime, there is an abrupt rise in η_{red} as the polymer concentration decreases; addition of salt gradually hinders this effect. At higher polymer concentrations, on the boundary between dilute and semidilute regimes, there is another rise of η_{red} with increasing polymer concentration, less sharp than in the dilute region, which is observed regardless of the presence of salt. A comparison between Fig. 4 and Fig. 1 shows that the steep increase at low polymer concentrations is the short chain counterpart of the Fuoss regime in the long chain case; the continuous line represents the Fuoss $\eta_{red} \sim C_p^{-1/2}$ and we see that the short chains have a much softer decay. The dashed line represents $\eta_{red} \sim C_p^{1/2}$, which describes the unentangled semidilute region in the case of long polyelectrolytes; it seems that, in this regime, short and long chains have comparable scaling laws, but this is beyond the scope of our work.

4.2 Reduced viscosity of solutions *versus* the Debye length

The reduced viscosity, defined in eqn (1), can be expressed as

$$\eta_{red} = \frac{\eta - \eta_s}{\rho C_p \eta_s}. \quad (7)$$

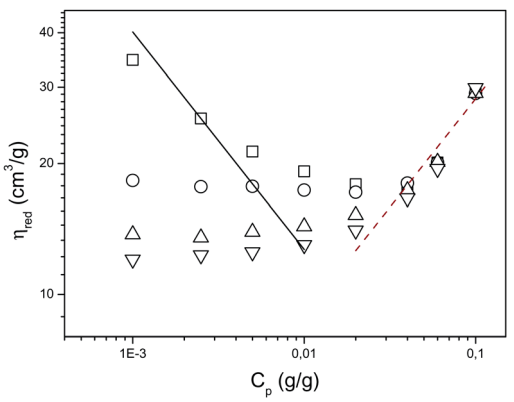

Fig. 4 Measured reduced viscosity as a function of polymer concentration at different salt concentrations. Squares: c_s = 0.00 mol l^{-1}; circles: c_s = 0.01 mol l^{-1}; up triangles: c_s = 0.05 mol l^{-1}; down triangles: c_s = 0.1 mol l^{-1}. Straight and dashed lines refer to $C_p^{-1/2}$ and $C_p^{1/2}$ dependences.

To characterize the importance of the electrostatic effect, we measured the variations of the reduced viscosity with the Debye length at different concentrations (Fig. 5). For each concentration, η_{red} increases linearly with λ_D. In the limit of vanishing polymer concentration, the straight lines have a common intercept at $\eta_{red} = 7.5$ cm^3 g^{-1}.

4.3 Discussion

Fig. 5 highlights the importance of the presence of charges on the styrene–maleic acid molecules. Only when the Debye length is very small, charges can be neglected and the viscosity of the solutions can be described as in neutral systems. In contrast, when the Debye length becomes larger, screening of the electrostatic charges becomes less efficient, which leads to an increase in the viscosity. To understand the origin of this increase in the viscosity, we are going to relate styrene–maleic acid molecules to charged colloidal rods and develop an approach inspired in the science of colloids. Classically the increase of viscosity in charged colloidal solutions is attributed to the so-called electroviscous effects.[19] Three different effects have been considered in the literature as follows. The primary electroviscous effect is due to the coupling between the double layers and the shear flow. The shear flow tends to distort the double layer around the rods. Electrical forces oppose this deformation. As a consequence, the ions in the double layers exert an additional friction everywhere through the suspending medium, including the region which flows around the particles. This friction increases the viscous dissipation and the viscosity. The secondary electroviscous effect refers to the increase of the viscosity as a result of screened electrostatic interactions between particles. In colloidal suspensions, the secondary electroviscous effect is particularly important at low ionic strength (*i.e.* at low particle concentrations) where the electrostatic interactions are able to modify the trajectories of approaching particles. Finally the tertiary electroviscous effect originates from changes that occur in the conformation of the polyelectrolytes. Next we estimate the relative importance of these effects.

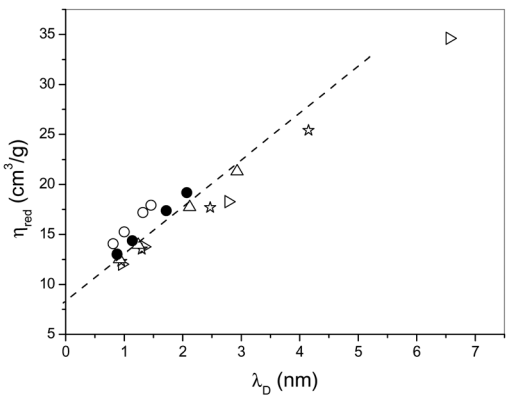

Fig. 5 Measured reduced viscosity *versus* the Debye length for various polymer concentrations. At every C_p, measurements at $c_s = 0.00$, 0.01, 0.05 and 0.1 mol l^{-1} are shown. Right triangles: $C_p = 0.001$ g g^{-1}; stars: $C_p = 0.0025$ g g^{-1}; up triangles: $C_p = 0.005$ g g^{-1}; filled circles: $C_p = 0.01$ g g^{-1} and empty circles: $C_p = 0.02$ g g^{-1}. The dashed line is drawn to show the linear dependence and intercept.

4.3.1 The primary electroviscous effect. Two non-dimensional numbers characterize the interplay between electrical forces, Brownian motion and shear flow: the electrical Hartmann number and the ion Peclet number. The electrical Hartamnn number expresses the competition between electrical and viscous forces,

$$\mathrm{He} = \frac{\Psi_0{}^2 \varepsilon}{\eta_s \mu k_B T}, \quad (8)$$

where μ is the ion mobility and $\Psi_0 = \Psi(r = b/2)$ is the electrostatic potential on the rod.†

When the Hartamnn number is small, the flow around the particles is not much modified by the electrical forces; the additional dissipation is negligible. When the Hartamnn number is large, the flow around the particles is strongly distorted by the electric field, which leads to a large primary electroviscous effect. Using the order of magnitude values of the various parameters in styrene–maleic acid solutions, *e.g.* $\Psi_0 \simeq 0.1$ *V*, $\mu k_B T \simeq 10^{-9}$ m^2 s^{-1} and $\eta_s \simeq 10^{-3}$ Pa s, one estimates that the Hartmann number is equal to 7. This value being larger than 1 indicates that the electric field is coupled to the shear flow with a strong effect on the system.

The ion Peclet number measures the extent to which the fluid motion disturbs the ionic cloud, against the Brownian forces that tend to restore equilibrium. It is defined as

$$\mathrm{Pe} = \frac{\kappa \lambda_D L}{\mu k_B T}, \quad (9)$$

where κ is the shear rate. Typical values $\lambda_D \simeq L$ and $\dot{\gamma} \simeq 1$ s^{-1} give an order of magnitude value for the ion Peclet number which is much smaller than 1, indicating that there is no permanent distortion of the ionic cloud due to shear flow.

In conclusion, we have the following picture. In styrene–maleic acid solutions, the ionic clouds around the rods modify the shear flow in their vicinity and create an additional source of viscous dissipation. The Brownian forces are sufficiently strong to restore equilibrium and prevent any permanent distortion of the double layer.

4.3.2 The secondary electroviscous effect. To evaluate the importance of the secondary electroviscous effect, it is useful to compare the Debye length λ_D (eqn (4)) with the characteristic distance between rods d. To estimate d, we assume that $d \simeq n^{-1/3}$. Fig. 6 shows a comparison between λ_D and d. We observe that the Debye length is significantly smaller than the distance between rods and we rule out the existence of any secondary electroviscous effect.

4.3.3 The tertiary electroviscous effect. Let us now determine whether there is a contribution to the viscosity coming from a change in rod conformation. In Fig. 5 we studied the

† An infinite rod creates a potential Ψ at a distance r:[20] $\Psi(r) = \frac{\lambda_q \lambda_D}{2\pi\varepsilon b} \frac{K_0(r/\lambda_D)}{K_1(b/\lambda_D)}$, where $\varepsilon = 6.9 \times 10^{-10}$ C^2 N^{-1}m^{-2} is the dielectric constant of water, λ_q is the charge density per unit length, λ_D is the Debye length, K_0 and K_1 are modified Bessel functions.

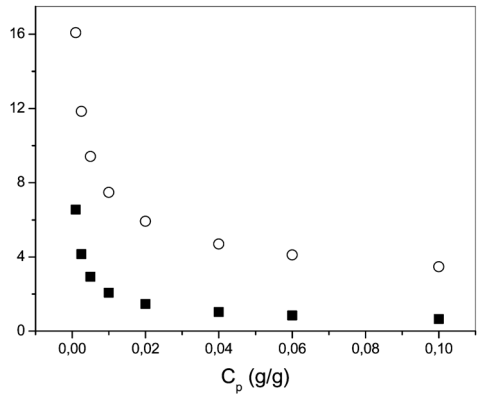

Fig. 6 Comparison between the distance between rods (empty circles) and the Debye length (filled squares) for various polymer concentrations. No added salt.

behavior of the reduced viscosity as a function of the Debye length; we observed that for small concentrations, in the limit of zero Debye length (*i.e.* charges completely screened) $\eta_{red} = 7.5$ cm^3 g^{-1}. Let us compare this value with the reduced viscosity of neutral rods of same length and aspect ratio,[9]

$$\eta_{red} = \frac{2\pi L^3}{45(\ln(L/b) - 0.8)} \frac{N_A}{M}. \quad (10)$$

For $L = 6.5$ nm and $L/b = 8$ we find $\eta_{red} = 7.2$ cm^3 g^{-1}. The agreement between these values shows that the degree of screening does not affect the conformation of the rods. The tertiary electroviscous effect is therefore negligible. Note that this situation is completely different from that investigated by Davis and Russel:[21] in potassium poly(styrenesulfonate) solutions, individual chains transform from compact coils to extended rods with decreasing ionic strength.

5 Theory

5.1 Modelling the primary electroviscous effects of charged rigid rods

The theoretical study of electroviscous effects in colloids is not a simple matter. The problems are easily formulated: coupled differential equations describing the electrostatics and hydrodynamics of the system. Nevertheless, they are hard to solve; an asymptotic analysis is not obvious and the numerical solution cannot always be obtained. As an example, Hinch and Sherwood[19] considered a suspension of spheres in the special case of thin double layers. They obtained local forms for the potential and ion densities, studied the fluid motion inside the charge cloud, and, by balancing the ion fluxes, obtained linear equations, which are examined in the case of low Hartmann number and asymptotic potentials. We choose to follow a different approach.

In the previous section we have shown that SMA molecules can be treated as charged rodlike particles immersed in an electrolyte. The extra contribution to the viscosity comes from the motion of the ions in the "rigid" double layer. To support this idea, we notice that in the dilute limit, the specific viscosity is a linear function of the effective volume fraction (Fig. 3); in the neutral analogue, the dependence of the specific viscosity on the bare volume fraction is linear with a logarithmic correction. We take into account the extra source of friction by considering an enlarged stiff neutral rod, consisting of the charged rod and its surrounding double layer.[8] With this picture, we calculate the total stress.

We thus consider a solution of neutral rods of enlarged length L^* and diameter b^* under excluded volume interactions. This picture maintains the shape of the double layer, replacing the effect of long range electrical forces by enhanced steric interactions. We obtain the final expression for the coefficient of viscosity which is very similar to the corresponding neutral system.

5.2 A general expression for the stress tensor in a dilute suspension of charged rigid rods

In our problem we have a short stiff polymer and we start by considering a theory for rodlike molecules. The first description was proposed by Simha;[22] we outline below a similar approach envisaged by Kirkwood[23] and reviewed by Doi and Edwards[9] for the fully extended chain model. In order to obtain an expression for the viscosity in the linear approximation, one looks for an expression for the total stress as a function of the fluid velocity gradient.

One considers a solution of rodlike polymers. Each rod has a length L^*, it consists of N beads of size b^*, so that $N = \frac{L^*}{b^*}$; this object is under an external potential V. Suppose it can be considered a Brownian particle immersed in a solvent with a viscosity η_s, flowing homogeneously with a velocity gradient κ. This approach handles both the dilute and semidilute regimes.

In the absence of external pressure the total stress can be written as

$$\sigma_{\alpha\beta} = \eta_s(\kappa_{\alpha\beta} + \kappa_{\beta\alpha}) + \sigma^p_{\alpha\beta}, \quad (11)$$

the first term represents the stress of the fluid in the absence of the polymer (*i.e.* due to the solvent only), the second term represents the excess stress due to the rods:

$$\sigma^p = \sigma^V + \sigma^E \quad (12)$$

The viscous stress σ^V is associated with hydrodynamic energy dissipation due to frictional forces; whereas the elastic stress σ^E is due to an additional energy loss associated with the Brownian motion of the rods.

For an incompressible fluid, weak velocity gradients and steady shear flow, the viscous stress is given by

$$\sigma^V_{\alpha\beta} = n \frac{\xi_r}{30}(\kappa_{\alpha\beta} + \kappa_{\beta\alpha}), \quad (13)$$

where ξ_r is the rod friction constant,

$$\xi_r = \frac{\pi\eta_s L^{*3}}{3\ln[(L^*/b^*) - 0.8]}. \quad (14)$$

Under the same conditions described above for eqn (13), we obtain:

$$\sigma^{E}_{\alpha\beta} = 3nk_BTS_{\alpha\beta} - n\,\langle(\mathbf{u}\times\mathscr{R}V_{rod})_\alpha u_\beta\rangle, \quad (15)$$

where T is the temperature, V_{rod} is the potential acting on the rod:

$$V_{rod} = \begin{cases} 0 & \text{in the dilute case} \\ V & \text{in the semidilute case} \end{cases}. \quad (16)$$

$\mathbf{u}$ is a unit vector along the rod and $\mathscr{R}$ is the rotational operator,

$$\mathscr{R} \equiv \mathbf{u}\times\frac{\partial}{\partial\mathbf{u}}. \quad (17)$$

The average $\langle\ldots\rangle$ is over the rod direction equilibrium distribution $\Psi(\mathbf{u};t)$, which satisfies

$$\frac{\partial\Psi}{\partial t} = D_r^*\mathscr{R}\cdot\left[\mathscr{R}\Psi + \frac{\Psi}{k_BT}\mathscr{R}V\right] - \mathscr{R}\cdot(\mathbf{u}\times\kappa\cdot\mathbf{u}\Psi), \quad (18)$$

where

$$D_r^* \simeq D_r = \frac{k_BT}{\xi_r} \quad (19)$$

is the rotational diffusion constant.‡

In eqn (15), $S_{\alpha\beta}$ is the orientational tensor,

$$S_{\alpha\beta} = \left\langle u_\alpha u_\beta - \frac{1}{3}\delta_{\alpha\beta}\right\rangle. \quad (20)$$

In what follows we replace the electrostatic potential V (eqn. (15) and (16)) by a self consistent potential U_{scf} describing the excluded volume interactions in a system of rescaled rods,

$$U_{scf}(\mathbf{u}) = nk_BT\int d\mathbf{u}'\delta(\mathbf{u},\mathbf{u}')\Psi(\mathbf{u}';t), \quad (21)$$

with

$$\delta(\mathbf{u},\mathbf{u}') = 2b^*L^{*2}|\mathbf{u}\times\mathbf{u}'|, \quad (22)$$

where L^* and b^* are the rescaled rod dimensions. We replace the expression for δ above by a function which also increases with the angle between $\mathbf{u}$ and $\mathbf{u}'$,

$$\delta(\mathbf{u},\mathbf{u}') = \text{const.} - \delta_1 b^*L^{*2}(\mathbf{u}\cdot\mathbf{u})^2, \quad (23)$$

where δ_1 is a numerical factor, while L^* and b^* are the rescaled rod dimensions. It is of the form of Mayer and Saupe interaction and allows eqn (21) to be solved exactly; on the other hand it brings a disadvantage to be discussed in the next section. It yields

$$U_{scf} = \text{const.} - \frac{3}{2}Uk_BTu_\alpha u_\beta S_{\alpha\beta}, \quad (24)$$

where U is proportional to nb^*L^{*2}.

In order to obtain $\sigma^{E}_{\alpha\beta}$, we need to evaluate the first and second terms on the RHS of eqn (15). We start by the second term,

$$n\langle(\mathbf{u}\times\mathscr{R}U_{scf})_\alpha u_\beta\rangle = 3nk_BTU[S_{\alpha\mu}\langle u_\mu u_\beta\rangle - S_{\mu\nu}\langle u_\mu u_\nu u_\alpha u_\beta\rangle]. \quad (25)$$

‡ $D_r^* = D_r[4/\pi\int d\mathbf{u}'\Psi(\mathbf{u}';t)|\mathbf{u}\times\mathbf{u}'|]^{-2}$. In the region of linear viscosity D_r^* can be replaced by D_r.

Because our system is isotropic, $S_{\alpha\beta}$ is small; to keep first order terms in $S_{\alpha\beta}$, we set $\langle u_\mu u_\nu u_\alpha u_\beta\rangle \simeq 1/15(\delta_{\mu\nu}\delta_{\alpha\beta} + \delta_{\mu\alpha}\delta_{\nu\beta} + \delta_{\mu\beta}\delta_{\nu\alpha})$ and obtain

$$n\left\langle\left(\mathbf{u}\times\mathscr{R}U_{scf}\right)_\alpha u_\beta\right\rangle = \frac{3}{5}nk_BTUS_{\alpha\beta}. \quad (26)$$

Next we consider the first term on the RHS of eqn (15) and look for an equation for $S_{\alpha\beta}$. Using the kinetic equation[9] for the orientational distribution function (eqn (18)), we obtain

$$\frac{\partial S_{\alpha\beta}}{\partial t} = -6D_r^*S_{\alpha\beta} + 6D_r^*U\left[S_{\alpha\mu}\langle u_\mu u_\beta\rangle - S_{\mu\nu}\langle u_\alpha u_\beta u_\mu u_\nu\rangle\right] + \kappa_{\alpha\mu}\langle u_\mu u_\beta\rangle + \kappa_{\beta\mu}\langle u_\mu u_\alpha\rangle - 2\kappa_{\mu\nu}\langle u_\alpha u_\beta u_\mu u_\nu\rangle. \quad (27)$$

Because we calculate up to first order in κ (linear viscosity), the same approximation for $\langle u_\mu u_\nu u_\alpha u_\beta\rangle$ above is used, yielding

$$\frac{\partial S_{\alpha\beta}}{\partial t} = -6D_r^*S_{\alpha\beta}\left[1 - \frac{U}{5}\right] + \frac{1}{5}(\kappa_{\alpha\beta} + \kappa_{\beta\alpha}). \quad (28)$$

We consider a simple shear flow

$$\kappa_{\alpha\beta} = \begin{cases} \kappa & \text{for } \alpha = x \text{ and } \beta = y \\ 0 & \text{otherwise} \end{cases}, \quad (29)$$

and eqn (28) leads to

$$S_{\alpha\beta} = \frac{1}{30D^*\left(1 - \frac{U}{5}\right)}. \quad (30)$$

Using eqn (15), (26) and (30), we arrive at the final expression for the elastic stress:

$$\sigma^{E}_{\alpha\beta} = \frac{nk_BT}{10D_r}\kappa. \quad (31)$$

Eqn (11)–(13) and (31) lead to the final expression for the coefficient of viscosity:

$$\eta = \eta_s + \eta_s\frac{2\pi nL^{*3}}{45\ln[(L^*/b^*) - 0.8]}. \quad (32)$$

The specific and reduced viscosities are given by:

$$\eta_{sp} = \frac{2\pi nL^{*3}}{45\ln[(L^*/b^*) - 0.8]} \quad (33)$$

and

$$\eta_{red} = \frac{N_A}{M}\frac{2\pi L^{*3}}{45\ln[(L^*/b^*) - 0.8]} \quad (34)$$

respectively. Eqn (33) and (34) are analogous to the case of neutral rods, with L and b replaced by L^* and b^* respectively. The viscosity is unaffected by the potential V_{rod}. The reason for that is cancellation in the sum of the first and the second term on the RHS of eqn (15). This is a feature of our approximation: the self consistent potential and the form of the excluded volume interaction (eqn (23)).

Using L and b rather than L^* and b^*, with $L/b = 8$, eqn (33) can be written as η_{sp}: 0.071 nL^{*3}. Moreover, from eqn (6), $\phi_{eff} = 0.524\ nL^{*3}$. Solving for nL^{*3}:

$$\eta_{sp} = 0.14\phi_{eff}, \quad (35)$$

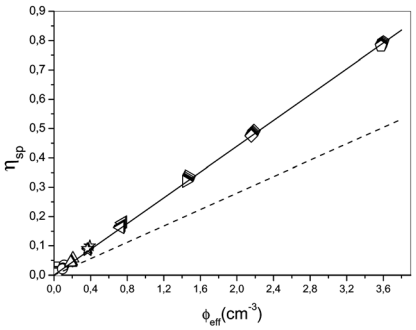

Fig. 7 Theoretical prediction: specific viscosity *versus* effective volume fraction. At every C_p, data for $c_s = 0.00$, 0.01, 0.05 and 0.1 mol l^{-1} are shown. Squares: $C_p = 0.001$ g g^{-1}; circles: $C_p = 0.0025$ g g^{-1}; up triangles: $C_p = 0.005$ g g^{-1}; stars: $C_p = 0.01$ g g^{-1}; left triangles: $C_p = 0.02$ g g^{-1}; right triangles: $C_p = 0.04$ g g^{-1}; diamonds: $C_p = 0.06$ g g^{-1} and pentagons: $C_p = 0.01$ g g^{-1}. The continuous line is a guide to the eye. The dashed line corresponds to eqn (35).

The theory predicts a unique functional form for η_{sp} as a function of ϕ_{eff} in both concentration regimes (eqn (33) and (35)). In order to check the universal behavior, we plot the specific viscosity (33) as a function of ϕ_{eff} (Fig. 7), with $L^* = L + \beta'\lambda_D$ and $b^* = b + \beta'\lambda_D$ and the simplified form, eqn (35). In order to optimize the fitting, we use $\beta' = 0.125$. The mismatch between solid (eqn (33)) and dashed (eqn (35)) lines shows that the latter is an oversimplified form of the former: the relevance of the electrostatic effects.

Fig. 8 shows our prediction for the reduced viscosity η_{red} (eqn (34)) as a function of the Debye length. λ_D. We notice that the data fall onto a single straight line, as opposed to the experiment, where each concentration has a different slope.

6 Conclusions

Fig. (7) reproduces qualitatively the universal behavior shown in Fig. (3). Our model predicts a single curve for all concentration regimes; nevertheless this is an artifact of our equations. It is well known that in the semidilute regime, the expression for D_r (eqn (35)) is not so simple; it may depend on n, L and b. Experimental and theoretical results question this point.[24,25] We predict a slope equal to 0.22 cm^3, much lower than 0.55 cm^3, of the dilute region of the experiment; possibly the expression for D_r, derived for the "shish-kebab" model, is not suitable for the SMA structure.

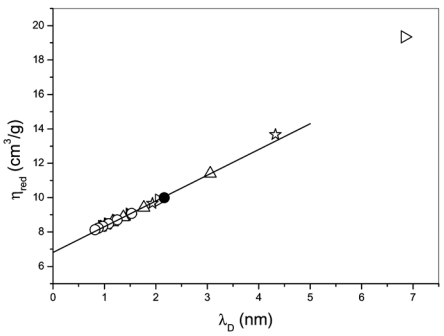

Fig. 8 Theoretical prediction: reduced viscosity *versus* Debye length for various polymer weight fractions. At every C_p, data for $c_s = 0.00$, 0.01, 0.05 and 0.1 mol l^{-1} are shown. Right triangles: $C_p = 0.001$ g g^{-1}; stars: $C_p = 0.0025$ g g^{-1}; up triangles: $C_p = 0.005$ g g^{-1}; filled circles: $C_p = 0.01$ g g^{-1} and empty circles: $C_p = 0.02$ g g^{-1}. The dashed line is drawn to show the linear dependence and the intercept.

The linear dependence of the reduced viscosity as a function of the Debye length (Fig. (5) and (8)) is nicely predicted by our model, but again with a quantitative discrepancy; the experiment gives a slope of 4.5 cm^3 g^{-1} nm^{-1}, whereas the theory gives 2.0 cm^3 g^{-1} nm^{-1}, probably for the same reason described above. Theoretically the intercept $\eta_{red}(0)$ is at 6.8 cm^3 g^{-1}, while experimentally the value is 7.5 cm^3 g^{-1}.

In general we observe qualitative agreement. The cancellation between Brownian motion and electrostatic potential effects is an artifact of our approach, nevertheless there must be some truth in it; a partial neutralization of physical effects actually occurs. A numerical solution of our equations using the real excluded volume potential could answer this question. A striking feature is that the experiment and theory are best fitted by the same value: $\beta = \beta'$.

A few questions remain open: (i) what model must be used to predict a suitable value for D_r in the dilute regime; (ii) it is possible to relate β to other model parameters to explain why they are the same. On the experimental side, we propose that measurement of viscosity as a function of the effective volume fraction as a route for obtaining D_r in the dilute and semidilute regimes (of course the correct relationship with ξ_r should be questioned).

From a broader perspective, fundamental questions remain open in the study of short polyelectrolytes. They concern the existence of a peak as in the case of long polyelectrolytes (under very dilute conditions) and the determination of scaling laws in the various concentration regimes.

Here we propose a model, where short polyelectrolytes are replaced by neutral rescaled rods; they consist of rods and a fraction of the surrounding ionic cloud. The neutral rods interact through an excluded volume potential of the Mayer and Saupe form. We conclude that in the dilute and semidilute regimes, the viscosity behavior of these short polyelectrolytes can be qualitatively described by our model.

Acknowledgements

This work was supported by the Capes-Cofecub project. One of us (D.I.) wishes to thank FUJB-UFRJ also for partial funding.

References

1 R. M. Fuoss, *J. Polym. Sci.*, 1948, **3**, 602–603.
2 R. M. Fuoss, *J. Polym. Sci.*, 1948, **3**, 603–604.
3 R. M. Fuoss, *Discuss. Faraday Soc.*, 1951, **11**, 125–134.
4 J. Yamanaka, H. Matsuoka, H. Kitano, H. Kitano, M. Hasegawa and N. Ise, *J. Am. Chem. Soc.*, 1990, **112**, 587–592.
5 D. C. Boris and R. H. Colby, *Macromolecules*, 1998, **31**, 5746–5755.

6 J.-L. Barrat and J.-F. Joanny, *Advances in Chemical Physics: Polymeric Systems*, 1996.
7 I. Piirma, *Polymeric Surfactants*, Marcel Dekker, Inc., New York, 1st edn, 1992.
8 A. M. Wierenga and A. P. Philipse, *Langmuir*, 1997, **13**, 4574–4582.
9 M. Doi and S. F. Edwards, *The Theory of Polymer Dynamics*, Oxford University Press, Oxford, 1st edn, 1986.
10 M. Doi, *J. Chem. Phys.*, 1983, **79**, 5080–5087.
11 M. W. Kim and D. G. Peiffer, *Europhys. Lett.*, 1988, **5**, 321–326.
12 R. F. Prini and A. E. Lagos, *J. Polym. Sci., Part A: Gen. Pap.*, 1964, **2**, 2917–2928.
13 H. Vink, *Polymer*, 1992, **33**, 3711–3716.
14 H. Eisenberg and J. Pouyet, *J. Polym. Sci.*, 1954, **13**, 85–91.
15 J. Cohen, Z. Priel and Y. Rabin, *J. Chem. Phys.*, 1988, **88**, 7111–7116.
16 A. V. Dobrynin and M. Rubinstein, *Prog. Polym. Sci.*, 2005, **30**, 1049–1118.
17 C. Oelschlaeger, M. C. P. Coelho and N. Willenbacher, *Biomacromolecules*, 2013, **14**, 3689–3696.
18 C. Dumousseaux, PhD thesis, Université Pierre et Marie Curie, Paris, 2000.
19 E. J. Hinch and J. D. Sherwood, *J. Fluid Mech.*, 1983, **132**, 337–347.
20 J. D. Sherwood, *J. Fluid Mech.*, 1981, **111**, 347–366.
21 R. M. Davis and W. B. Russel, *Macromolecules*, 1987, **20**, 518–525.
22 R. M. Simha, *J. Phys. Chem.*, 1940, **44**, 25–34.
23 J. G. Kirkwood, *Documents on Modern Physics*, 1967.
24 Y. Kori, N. Ookubo, R. Hayakawa and Y. Wada, *J. Polym. Sci.*, 1982, **20**, 2111–2124.
25 S. Jain and C. Cohen, *Macromolecules*, 1981, **14**, 759–765.